JOURNAL OF
biomaterials
applications

Article

Journal of Biomaterials Applications
0(0) 1–15

DOI: 10.1177/0885328215601938
jba.sagepub.com
SAGE

Brushite-based calcium phosphate cement with multichannel hydroxyapatite granule loading for improved bone regeneration

Swapan Kumar Sarkar[1], Byung Yeol Lee[2], Andrew Reyas Padalhin[3], Avik Sarker[3], Nathaniel Carpena[1], Boram Kim[3], Kallyanshish Paul[3], Hwan Jun Choi[4], Sang-Ho Bae[5] and Byong Taek Lee[1,3]

Abstract

In this work, we report brushite-based calcium phosphate cement (CPC) system to enhance the in vivo biodegradation and tissue in-growth by incorporation of micro-channeled hydroxyapatite (HAp) granule and silicon and sodium addition in calcium phosphate precursor powder. Sodium- and silicon-rich calcium phosphate powder with predominantly tri calcium phosphate (TCP) phase was synthesized by an inexpensive wet chemical route to react with mono calcium phosphate monohydrate (MCPM) for making the CPC. TCP nanopowder also served as a packing filler and moderator of the reaction kinetics of the setting mechanism. Strong sintered cylindrical HAp granules were prepared by fibrous monolithic (FM) process, which is 800 μm in diameter and have seven micro-channels. Acid sodium pyrophosphate and sodium citrate solution was used as the liquid component which acted as a homogenizer and setting time retarder. The granules accelerated the degradation of the brushite cement matrix as well as improved the bone tissue in-growth by permitting an easy access to the interior of the CPC through the micro-channels. The addition of micro-channeled granule in the CPC introduced porosity without sacrificing much of its compressive strength. In vivo investigation by creating a critical size defect in the femur head of a rabbit model for 1 and 2 months showed excellent bone in-growth through the micro-channels. The granules enhanced the implant degradation behavior and bone regeneration in the implanted area was significantly improved after two months of implantation.

Keywords

Calcium phosphate cement, silicon, biodegradability, porosity, porous granule

Introduction

During the past few decades, there have been major advances in the development of ceramic-based biomedical materials that have been exploited to augment the repair of damaged human hard tissue. Particularly, with the advent of minimally invasive surgery techniques, materials with self-setting properties have been investigated for clinical use.[1–3] Despite current limitations of these minimally invasive systems that include lack of porosity and restricted working time during the application, these materials can be beneficial when used in specific conditions that best serve the purpose.

[1]Institute of Tissue Regeneration, College of Medicine, Soonchunhyang University, Cheonan, South Korea
[2]InoBone Corporate R&D Center, Soonchunhyang University, Asan-si, South Korea
[3]Department of Regenerative Medicine, College of Medicine, Soonchunhyang University, Cheonan, South Korea
[4]Department of Plastic and Reconstructive Surgery, College of Medicine, Soonchunhyang University Hospital, Cheonan, Republic of Korea
[5]Department of Surgery, College of Medicine, Soonchunhyang University Hospital, Cheonan, Republic of Korea

Corresponding author:
Byong-Taek Lee, Soonchunhyang University, Ssangyoung-Dong, Chungnam Cheonan City 330-090, Republic of Korea.
Email: lbt@sch.ac.kr

The current gold standard for bone reconstruction is the autologous bone graft. Disadvantages include the need for an additional prerequisite surgery at the donor site, limited availability, unfavorable shape, donor site morbidity, and low resorption rate of the graft.[4] Allografts are the next choice, but this option is hindered by limited supply and potential risks of disease transmission and possible immunorejection. Current artificial orthopedic implant materials that include those based on sintered calcium phosphate (CP) lack a suitable universal implant preform to fit into the surgical site. Nonconformity of the implant to the defect site can increase bone loss, cause trauma to the surrounding tissue, poor bone regeneration and prolong surgery time. Reworking of the defect site may additionally be required to fit the self-sintered ceramic scaffold. Bone substitute materials with a moldable paste-like consistency that can harden at the defect site in situ are a convenient and attractive alternative to sintered bone filling materials.

Chow and Brown[5] first introduced calcium phosphate cement (CPC). CPCs have subsequently attracted much interest because of their ease of application in the defect site, potential tissue compatibility and eventual ossification and bone reconstruction.[6,7] CPCs can be easily applied in the defect site to completely fill the defect zone,[8] after which they self-harden to form biologically relevant hydroxyapatite (HAp) or brushite. Both have excellent osteoconductivity and bone-replacement abilities.[9–16] In their current formulation, CPCs consist of a powder containing one or more solid compound of CP salts and a liquid component. Mixing of the powder and liquid in an appropriate ratio yields a moldable or injectable paste that can be applied to the defect, and which sets at room or body temperature by the entanglement of the crystals precipitated within the paste.[17]

The application advantages are tempered by several issues that hinder the potential of CPCs as a bone tissue regeneration option. Apatite-based CPC made by reacting tetra-calcium phosphate (TTCP) and di-calcium phosphate di-hydrate (DCPD), which sets to form a mass of HAp, is strong but resorbs very slowly in physiological conditions. Brushite-based CPC, which is made by reacting acidic mono-calcium phosphate monohydrate (MCPM) with tri-calcium phosphate (TCP), degrades faster than apatite CPC but is not comparatively as strong and biocompatible. Moreover, the inherent lack of interconnected porosity significantly decreases the potential of tissue in-growth. Even though the set mass of the applied CPC has some micro-porosity, they are not interconnected and the pore size and pore size distribution are largely unfavorable for the bone tissue in-growth. More extensive porosity and pore size in the range of 100–500 μm are desired for rapid osteoconduction and remineralization.[18] CPC-based bone substitutes lack this interconnection and well-developed porosity, and primarily depend on surface degradation through physicochemical processes or cellular interaction for bone in-growth. Both of these processes are relatively slow and may require months or years for a brushite-based CPC and even longer for an apatite CPC. In bone healing, degradation of the CPC is pivotal for the complete ossification of the implant site. This has prompted many recent studies to improve the inherent biocompatibility of the brushite-based CPC by incorporating a secondary degradable phase with favorable size distribution to create porosity.[19]

The addition of a secondary degradable polymer within the CPC matrix can significantly alter the physical–mechanical performance of the CPC due to the drastically dissimilar elastic modulus of the two. Moreover, the creation of cell in-growth passages through degradation of polymers is a slow process requiring simultaneous degradation and removal of degraded products from the site of consideration prior to tissue in-growth. This strongly depends on the inherent degradation behavior of the polymer itself and may not be synchronized with that of the bone tissue in-growth. Thus, it may not be as optimized as compared to the readily available porous interior found in porous scaffolds in terms or cellular bone in-growth.

Based on the above considerations, it is logical to incorporate a bioceramic-based porous granule within the brushite-based moldable CPC. A strong sintered HAp porous granule with favorable pore size can provide passage for cell in-growth. Furthermore, HAp may promote interfacial bonding between the CPC matrix and the granule surface due to the same reaction that hardens the CPC. As the sintered HAp is mechanically stronger than the hardened CPC, the granules can mechanically reinforce the CPC, with the load being transferred into the granules from the matrix. This can potentially reduce the adverse effect of weakening of CPC that is obvious in incorporating polymer porogen materials or any kind of porosity introduction. We have previously developed multi-channeled granular bone substitutes of HAp and biphasic CPs.[20] The granules made by fibrous monolithic process harbor seven holes in a tight geometry. The sintered granules are strong and augment bone defect healing.[21] The present study used these micro-channeled granules along with a brushite-based CPC to impart porosity and mechanical stability to the later. This multi-channeled cylindrical granular bone substitute has been introduced in South Korea for clinical application after due approvals. It has seven through channels with pore size ranging from 150 to 200 μm and has a diameter of around 1 mm. Thickness of the HAp

struts for the cylindrical granule is less than 200 µm which indicates a potential short time biodegradation of the granule.

Silicon is an essential element for bone and cartilage development. Silicon-enriched regions are most abundant on the mineralization front of growing bone where osteoblastic activity is pronounced.[22–24] Silicon is essential to the normal development of the glycosaminoglycan network in the extracellular matrix and is a crucial structure/function regulator of these molecules. The bimolecular activity of osteoblasts in regulating the expression of several genes, including key osteoblastic markers, cell cycle regulators and extracellular matrix proteins has been reported to be profoundly influenced by silicon-rich degradation products (predominantly silicic acid) from bioglass.[25] Thus, silicon incorporation is one way to inherently modify the material of consideration, such as HAp and TCP, to improve biocompatibility and osteogenic potential. Calcium silicate-based cement has already been found as an excellent endodontic sealer.[26] Relatively longer setting time of this system, however, is not suitable for bone cement application. Thus, there exists a scope for combining the aspects of these two types of cementacious materials in the application of bone cement, and our current work focuses on this aspect to fabricate a more biocompatible and biodegradable CPC system.

In this study, we introduce silicon-rich calcium phosphate-based CPC as a new hydraulic cementacious material. This material accelerates the setting reaction of the cement and significantly improves bone regeneration. Micro-channeled granules incorporated within the CPC matrix introduce porosity which enhances cell in-growth and *in vivo* biodegradation.

Materials and methods

Silicon rich CP powder manufacture

A hydrothermal synthesis rout assisted by microwave heating was used to prepare silicon and sodium incorporated CP powder. Calcium nitrate tetra-hydrate (Samchun Pure Chemicals), di-ammonium hydrogen phosphate (Samchun Pure Chemicals), and sodium silicate solution (35–38% SiO_2 and 17–18% Na_2O, Samchun Pure Chemicals) were the raw materials. The chemicals were separately dissolved in warm water (60°C). Di-ammonium hydrogen phosphate solution and sodium silicate solution were homogenized and quickly added to the calcium nitrate solution at 60°C and stirred vigorously with an overhead stirrer. The pH of the solution was maintained at 9 adding saturated ammonia solution. The resulting slurry was stirred for 4 hours at 60°C and transferred to a microwave oven and heated for 40 min (70% active heating for 2 minutes and 30% intervening intervals). The slurry was transferred to a drying oven and kept for several days at 80°C for complete drying. The dried lumps were crushed, homogenized and sieved through a 100 µm pore size sieve. The material was calcined at 1200°C for 2 h, crushed, ground, and sieved. The resulting powder was used for making CPC. The mole ratio of NaH_2PO_4:$Ca(NO_3)_2$.$4H_2O$:Na_2O.(SiO_2):$(NH_4)_2HPO_4$ was 0.2:1.4:0.1:0.7 for silicon rich CP synthesis.

Preparation of CPC

A liquid solution was mixed with a powder mix. The solution contained 1 molar tri-sodium citrate solution and 4% (w/w) di-sodium di-hydrogen pyrophosphate. The concentration was settled after initial trial runs with varying concentration to obtain paste-like settable mass. Samples (CPC bone substitutes) were prepared by mixing the liquid phase with the powder phase with the help of a spatula. The powder components in the CPC were varied to optimize the setting time and pH. We investigated three compositions and the optimized CPC (liquid/powder = 0.4) was used for loading the micro-channel granules. The liquid solution was mixed with the premixed powder component and vigorously stirred for less than a minute. The paste quickly became fluid and malleable. Micro-channel granules were added to the paste and mixed quickly to prepare granule-loaded CPC. No extra liquid was added while granule loading, as the large granules minimally affected fluidity of mixed CPC. The sticky CPC mass was quickly transferred to polypropylene molds 8 mm in diameter and 5 mm in length, and kept in a chamber at 37°C and 100% relative humidity. The compositions of the liquid and solid phase of different CPCs are shown in Table 1. Based on the composition, the CPCs were named as CPC1, CPC2, CPC3 (optimized CPC without granules), and CPC4 (optimized CPC with micro-channel granules).

Phase and composition analysis

Phases in the powders and cements were characterized by X-ray diffraction (D/Max-250; Rigaku, Japan) at 40 kV and 200 mA with a scan rate of 2°/min, and using energy dispersive spectroscopy (EDS; Oxford Instruments, UK). The set samples were ground prior to analysis. Area EDS was taken for multiple instances from the platinum sputter-coated sample during scanning electron microscopy (SEM) observation. Both area EDS for composition analysis and elemental mapping EDS for spatial distribution of the constituent elements were observed.

Table 1. CPC compositions.

Sample	Na-Si-CaP (gm)	TCP (gm)	MCPM (gm)	Granule (gm)	Na_3 Ct solution (M)	$Na_2H_2P_2O_7$ solution (%, w/v)	L/P
CPC1	1.00	0	0.50	0	1	4	0.4
CPC2	0.50	0.50	0.50	0	1	4	0.4
CPC3	0.50	0.50	0.35	0	1	4	0.4
CPC4	0.50	0.50	0.35	0.67	1	4	0.4

Morphology of cements

After setting, powders and cements were observed by SEM using a JSM-635 apparatus (JEOL, Japan) with a platinum sputter coating. Each sample was polished on sintered Alumina flat surface and dried prior to observation. For SEM observation of in vivo tissue sections, formalin-fixed, extracted bone segments were decalcified in 5% nitric acid for 36 h and dehydrated in a series of ethanol solution increasing from 50% to 100% overnight. Each dehydrated section was kept in xylene for 3 h to remove alcohol. It was then paraffin-embedded and polished in a diamond polishing plate. Deparaffinization of the polished tissue block was done afterwards in xylene. The deparaffinized block was dried at room temperature and freeze-dried for 1 day prior to SEM observation.

Setting time measurement

Setting times of the samples were measured using the Gilmore needle method. A cement specimen, kept at 100% relative humidity at 37°C, was considered set when a 400 g mass loaded to a needle with a tip diameter of 1 mm failed to make a perceptible indentation on the surface of the cement. For each sample category, at least five measurements were taken and then averaged.

Measurement of pH of the set sample

Two of the precursor materials were acidic (MCPM and acid sodium pyrophosphate). Although trisodium citrate was used as a retardant and buffer for acidity control, and the final pH of fabricated CPC was still low. This low pH is a perquisite for the brushite crystal precipitation and hence setting mechanism. However, the initial acidic microenvironment is not favorable for the surrounding tissue and even could be toxic. Thus, we evaluate the change of pH of the set samples with time. The set CPC sample was dipped in water and the solution pH was measured. The set CPCs were molded in a cylindrical shape of uniform size and were kept in distilled water in a sealed tube at 37°C. The matrix phase of CPC3 and CPC4 is the same and pH change is due to the ion release from the matrix phase. We measured the pH change for CPC3 composition only. The set samples with 8 mm diameter and 5 mm length were immersed in 10 ml distilled water and the pH was measured after stipulated time span. To evaluate both static condition and dynamic condition, two sets of samples were immersed in deionized water. In one set, solvent was replenished every 6 hours for first the 24 h and subsequently every 12 h for 1 week. The other set did not experience any change in solvent during the entire one-week time period.

Compressive strength measurement

Cement samples were molded into cylindrical tubes measuring 5 mm in height and 8 mm in diameter. The specimens were incubated in a closed vessel at 37°C and 100% relative humidity for 1 and 7 days, after which compressive strength was measured ($n = 5$) using a computer-controlled Universal Testing Machine (R&B, Korea) at a crosshead speed of 0.5 mm/min. At least five specimens were used for measuring the compressive strength and the average value was taken.

In vivo *testing*

Implantation of CPC in rabbit femur. New Zealand white rabbits were used for in vivo implantation for evaluation of control, CPC3 and CPC4. For each sample, three rabbits were operated for a single time span. Implantation was duplicated for two time spans (4 and 8 weeks). The protocol for the care and use of laboratory animals was approved by the Animal Ethical Committee of Soonchunhyang University and was duly observed. The rabbits (weighing around 3 kg) were individually housed in stainless-steel cages and taken care of. A combination of 1.3 ml ketamine (100 mg ml^{-1}, Ketara; Yuhan, Korea) and 0.2 ml xylazine (7 mg kg^{-1} body wt., Rompun; Bayer Korea, Korea) was used for general anesthesia, which was administered by intramuscular injection. The surgical areas were shaved and the skin was treated with

iodine solution. After exposure of the femoral head, an 8 mm diameter and 5 mm deep cylindrical defect was created using a trephine drill. The resulting defect was filled with the CPC3 or CPC4 that had been prepared immediately and applied to the defect prior to the start of cement setting. Control defects without any further treatment were used as negative control. After surgery, the surgical sites were closed in layers and sutured. Antibiotic (Baytril, Bayer Korea) was injected intramuscularly for three days and the sutured area was treated with iodine to prevent post-surgical infection. The animals were sacrificed by intravenous injections of air under general anesthesia after 4 and 8 weeks. Femur head was isolated for micro-computed tomography (CT) and histological analysis.

Micro-CT analysis. The extracted bone segment of the femur head was fixed in 10% formalin solution. Micro-CT of the harvested bone section was done using a model 1076 apparatus (Skyscan, Belgium) to observe new bone formation. Each sample was fixed on the object stage, and imaging was performed on the sample with 360° of rotation with an exposure time of 20 min. Micro-CT images were reconstructed over the region of interest (ROI) using CTAn (Skyscan) and CTVol (Skyscan) depicting the three-dimensional interior of the defect zone. Quantification of percent bone volume (BV/TV, %) was calculated from total defect volume (TV) and bone volume (BV).

Histological analysis. After the micro-CT analysis, the formalin-fixed bone sections were decalcified using 5% nitric acid for 36 hours and then washed extensively to remove any remaining acids. Sections were then dehydrated using an ethanol series (70–100%) and residual ethanol was removed by dipping in xylene. Specimens were cleared of xylene by dipping in molten paraffin wax at 60°C and then embedded in paraffin. Tissue slices $5 \pm 2\,\mu m$ in thickness were cut using a microtome (Thermo-Scientific, USA) and the sections were stained by hematoxylin and eosin (H&E) and Masson's trichrome stain. Tissue sections were viewed with a BX53 light microscope (Olympus, Japan) and photographed with a model DP72 camera (Olympus). Images were analyzed using accompanying Cellsens software.

Statistical analysis

All tests were done using at least five replicates, unless otherwise stated. Values were expressed as the mean and standard deviation of the measurements. Experimental results were analyzed for significance with Student's t-test, with a confidence level of $P \geq 0.05$, using Microsoft Excel 2010.

Results

Synthesis of sodium-silicon-CP powder

The as-synthesized powders were softly agglomerated. After crushing to fine particle and calcinations, hard agglomerates were formed again. Grinding and sieving produced a typical particle size $<100\,\mu m$ (Supplementary data). The calcined powders showed peaks primarily associated with calcium phosphate silicate, $Ca_5(PO_4)_2SiO_4$ (ICDD card no. 400393), as shown in Figure 1(c). Peaks of HAp (ICDD card no. 10860740) and dicalcium silicate, $Ca_2(SiO_4)$ (ICDD card no. 10709857), were also observed. A trace level of sodium hexametaphosphate and trisodium phosphate was detected in crystallographic observation.

Phase and morphology observations

After setting, CPC3 turned to the brushite (ICDD card no. 10743640) and monetite (ICDD card no. 10700360) phase with a minor presence of HAp (ICDD card no. 10759526). No unreacted component of residual TCP, MCPM or calcium phosphate silicate was found. This indicated the complete transformation of the CPC to the biologically relevant brushite phase. The emergence of monetite is largely due to the loosening of crystallization water during the drying of set sample prior to grinding for XRD observation. The advent of the dicalcium silicate (DCS) phase (ICDD card no. 240234) in the set cement was an indication of the reaction of the calcium phosphate silicate phase in the cement premix to precipitate calcium silicate crystals. The set mass has much less-pronounced crystallinity compared to the precursor compounds. The amorphous nature of the set mass was evident from the bulging of the peaks at around 35–35° and again at 38–45° of 2θ values. Figure 2(a), (d) and (e) depicts the surface morphology of both types of bone substitutes after setting. Figure 2(a) depicts a low magnification SEM image of Frabone-loaded CPC4. The porous channels were unblocked by the CPC paste and were open during the mixing process. The EDS profiles for the CPC matrix and Frabone are given in Figure 2(b) and (c), respectively. The elemental composition showed the relevant elemental peaks for both. Figure 2(d) shows a higher magnification of the CPC-Frabone interface. The interaction of the surfaces was very active and a strongly adhered Frabone–CPC contact was observed. Figure 2(e) shows a representative high magnification SEM of the CPC matrix common to both CPC 3 and CPC 4. The dense microstructure of the set sample is evident. The particle size of the set CPC differed from the precursor powders, indicating a strong interaction between the reactant. Brushite crystals precipitated with a homogeneous distribution. No significant

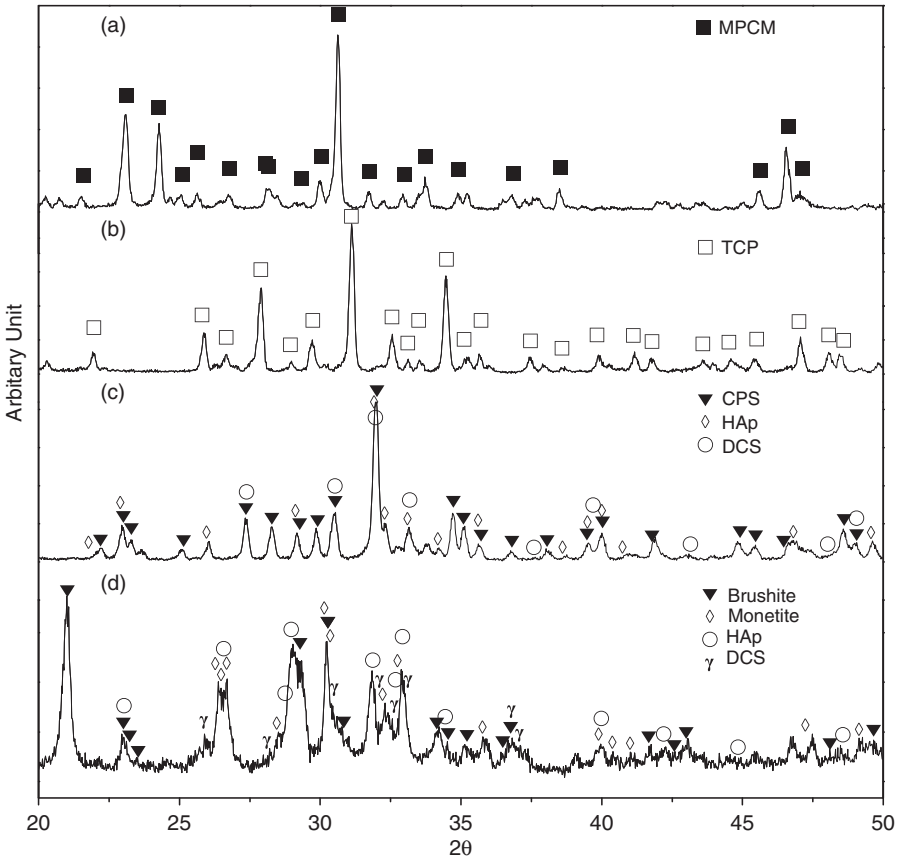

Figure 1. XRD profiles for the CPC system. Individual components (a–c) of the cement before mixing and (d) set sample after one week.

micro-porosity was observed in the microstructure. Elemental EDS mapping of the CPC as shown in SEM in Figure 2(e) is summarized in Figure 2(f) and (i) for silicon, sodium, calcium, and phosphorus, respectively. As evident in Figure 2(h) and (i), calcium and phosphorous were omnipresent, being the common elements for all three major precursors. However, the distribution of silicon was spatially different (Figure 2f, due to the separate precipitation of the silicon-rich phase in the CPC matrix as evident from XRD data (Figure 1d). However, the weak XRD peak profile also suggests that the phase predominantly precipitates in an amorphous phase. This in turn enhances the possibility of silicon bioavailability as evident in melt-derived and sol-gel-derived bioglass materials.

Setting time

The prepared sodium-silicon-CP phase was very reactive and, when used with MCPM in a 2:1 weight ratio, started hardening immediately as exemplified in the CPC1 composition in Figure 3(a). This weight ratio was approximately close to the stoichiometric molar ratio of TCP and MCPM required for formation of brushite. Adding 50 wt% nanocrystalline TCP slightly increased the setting time (CPC2 in Figure 3a). The setting time delayed significantly when the MCPM content was decreased in CPC3. Further decrease of MCPM content delayed the setting time but with the penalty of decreased mechanical property. The TCP nanopowders acted as a reaction moderator and enhancer for particle packing and dispersion of the solid phase due to the nano size. This markedly improved the handling properties and consistency of the mixed putty. This was necessary for incorporating the relatively large granules with the mixed cement to make the end product. $Na_2H_2P_2O_7$ in the liquid was chosen to delay the setting process by slowing the reaction. However, we did not use the commonly used $Na_4P_2O_7$ as this would tend to raise the pH of the cement mix. Usually, brushite crystals are precipitated in the reaction of CP salts at a pH <5. Incorporation of granules in the cement mix slightly decreased the setting time as evident for CPC4 (Figure 3a). The delay in setting time was due to the addition of more solid phase to the mix. The higher content of granule loading

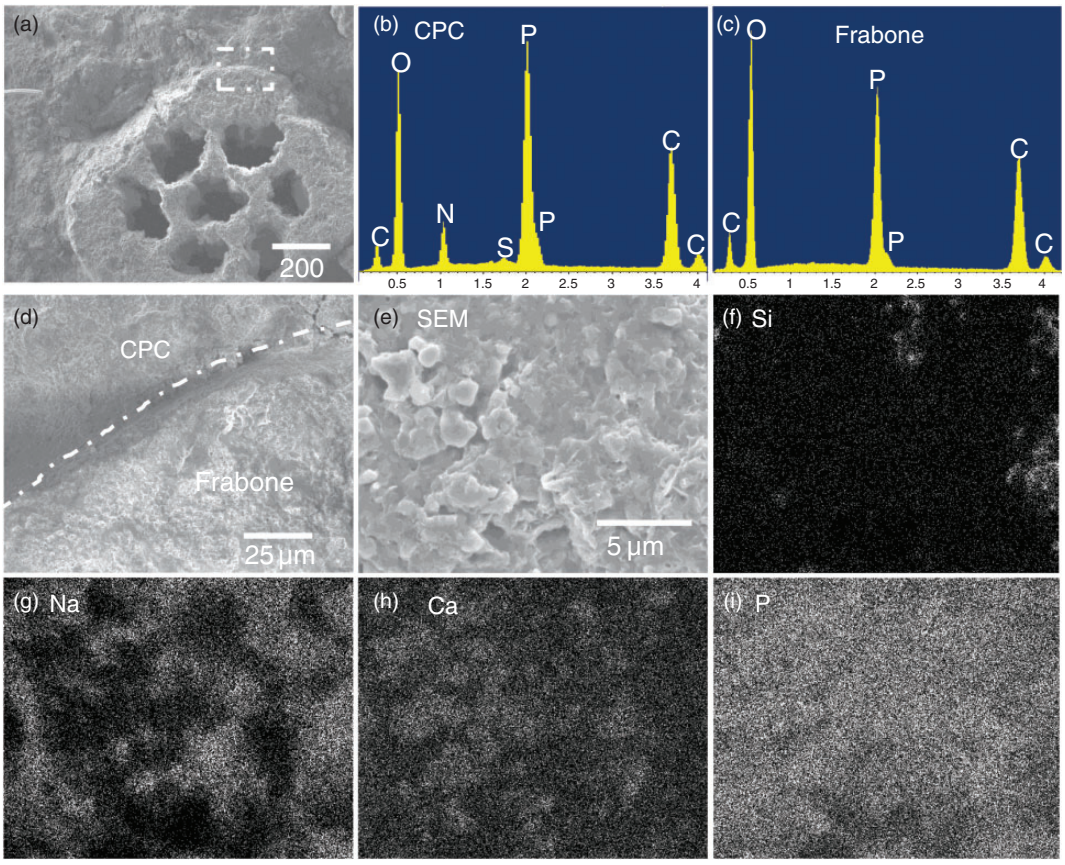

Figure 2. SEM images of granule-loaded IBS 4 after one day of setting. (a) Low magnification SEM image and EDS profile for the (b) CPC matrix and (c) Frabone. (d) High magnification interface SEM image. (e) High magnification SEM image from the set CPC. EDS mapping for (f) Si, (g) Na, (h) Ca and (i) P from the same area shown in (e). C=calcium, N= sodium, O = oxygen, S = silicon, P = phosphorous.

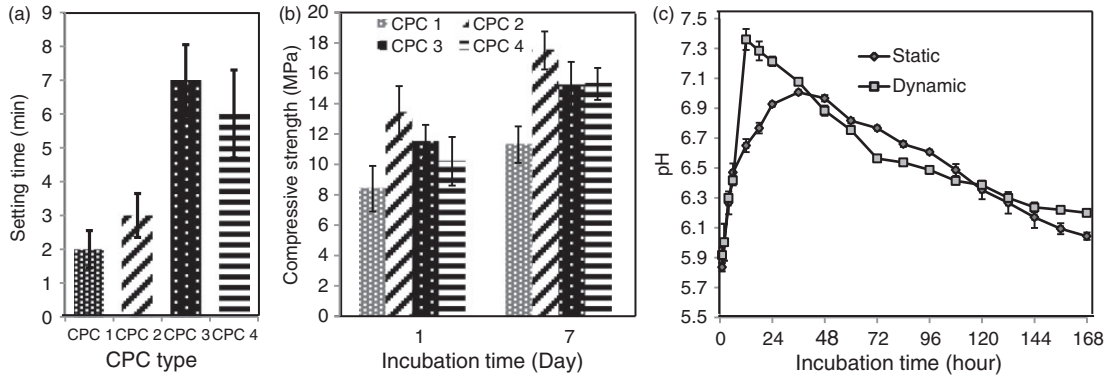

Figure 3. (a) Setting time of the CPC systems, (b) compressive strength of the CPC systems after one and seven days of incubation at 37°C in saturated humidity. (c) pH of the immersion solution for seven days of incubation in 37? day for CPC3 and CPC4 in static and dynamic conditions.

also caused a mechanical interlocking that prevented the dipping of the Gilmore needle apparatus. As much as 50% of the increase in dry weight of the cement solid phase by the addition of granule was not associated with a change in liquid content, which increased the actual liquid to solid ratio of the formulation. This basically made the actual liquid-to-solid ratio 0.26. The consistency of the paste was not altered significantly by this, as addition of the granules had little to do with the microenvironment where the precursor powders of sodium-silicon-CP, TCP, and MCPM interacted with the liquid phase. However, the

mechanical interlocking between large granules was evident and the workability was slightly decreased, albeit still application as putty to the defect site within the workable time prior to setting.

Mechanical strength

The compressive strengths of the set cements are shown in Figure 3(c). The addition of TCP nano-powder significantly increased the compressive strength at day 1 and 7 when incubated in a saturated enclosure at 37°C. However, decrease in MCPM content from CPC1 to CPC2 decreased the compressive strength. The compressive strength values were not as high as many other brushite-based bone cement systems currently being reported, but were adequate as a bone substitute material. After addition of the granules, the compressive strengths were slightly decreased in CPC4 compared to the granule less CPC3 after one day of incubation. Loading a high content of granular phase in a paste-like consistency significantly altered the mixing condition and particle packing of the CPC matrix. Without the granules, the putty-like consistency was easy to mold and compact, which was not the case when granules were present. However, the compressive strength gradually improved as the incubation time extended for seven days. Although the increment was not significantly different, it was evidence of the reinforcing effect of the granules. The sintered and strong granules in the CPC matrix had strong interfacial bonding with the granular surface and helped to compensate the strength decrease.

pH change

The change in pH with time for the CPC3 compositions for 1 week is depicted in Figure 3(c). After immersion, the pH of the solution drastically decreases initially and stabilizes to 5.8 ± 0.06. However, it starts to increase thereafter and continues to increase up to 7 for the static condition in 36 h and then shows a declining trend. In the dynamic condition, however, the pH is increased to 7.36 ± 0.08 in 12 h and then decreased continuously until 7 days. In the dynamic condition, we replenished the solution after every 6 h for the first 24 h due to the rapid change in pH. Interestingly, the pH showed a higher value compared to the static condition. This implies that the initial ion release from the acidic phase is much more pronounced which is counterbalanced by the basic ions. However, after 36 h in both cases, the pH starts decreasing slowly and continues to decrease until the seventh day. The initial spike of the pH can be attributed to the high influx of sodium ions from the matrix of the CPC. However, as time goes by the diffusion rate is decreased and the main component of the CPC matrix, the brushite phase, degrades considerably and changes the ion balance in favor of lower pH. The initial pH spike is a very favorable aspect for initial cell attachment and adhesion for cellular activity to start. This also potentially affects the initial inflammatory reaction in favor of cell-CPC interaction.

Invivo *biocompatibility*

Micro-CT observation. Figure 4 presents a three-dimensional reconstructed model of the cross section of femur head where the defects were drilled and CPC was implanted. From the images, the mid-section of the implant was selected as the top surface. Figure 4(a) and (b) is from the control defect after 1 month of implantation and Figure 4(c) and (d) is after 2 months of implantation. Femur head section after 1 month of implantation is shown in Figure 4(e) revealing CPC3 implanted critical defect. The implanted defect zone is shown in enlarged view in Figure 4 (f) where the unresorbed CPC3 is shown in pink color. Figure 4(g) and (h) depicts the femur head section and implanted defect zone, respectively, after 2 months of implantation for the CPC3 composition. From the micro-CT models, it is clear that the CPC3 underwent significant degradation, especially near the surface after 2 months of implantation. The degraded portion was filled with new bone as confirmed by the contrast similarity between the native bone and the space filled by the CPC3 degradation. Figure 4(i) shows the micro-CT model of the femur head section after one month where CPC4 composition was implanted in the drilled defect. Figure 4(j) shows the enlarged view of the implanted defect zone. Figure 4(k) and (l) presents micro-CT images of femur head section and implanted defect zone, respectively, for CPC4 after two months of implantation. The improvement of degradation and bone in-growth for the granule incorporated CPC4 was visually apparent. Degradation and bone in-growth were observed both after one and two months. After two months, the bone degradation was directed inward from all directions of the implant. However, as expected, the sintered granules were intact without any sign of degradation. Quantitative evaluation of the bone volume compared to the total volume of the defect zone is provided in Figure 5. Compared to control, percent BV/TV was higher after one month of implantation, although the difference was not statistically significant. On the other hand, after two months of implantation, the percent BV/TV was significantly different in the case of CPC3 and CPC4, with the latter showing increased bone formation behavior compared to control and CPC3. This indicates that use of porous granule in a CPC matrix

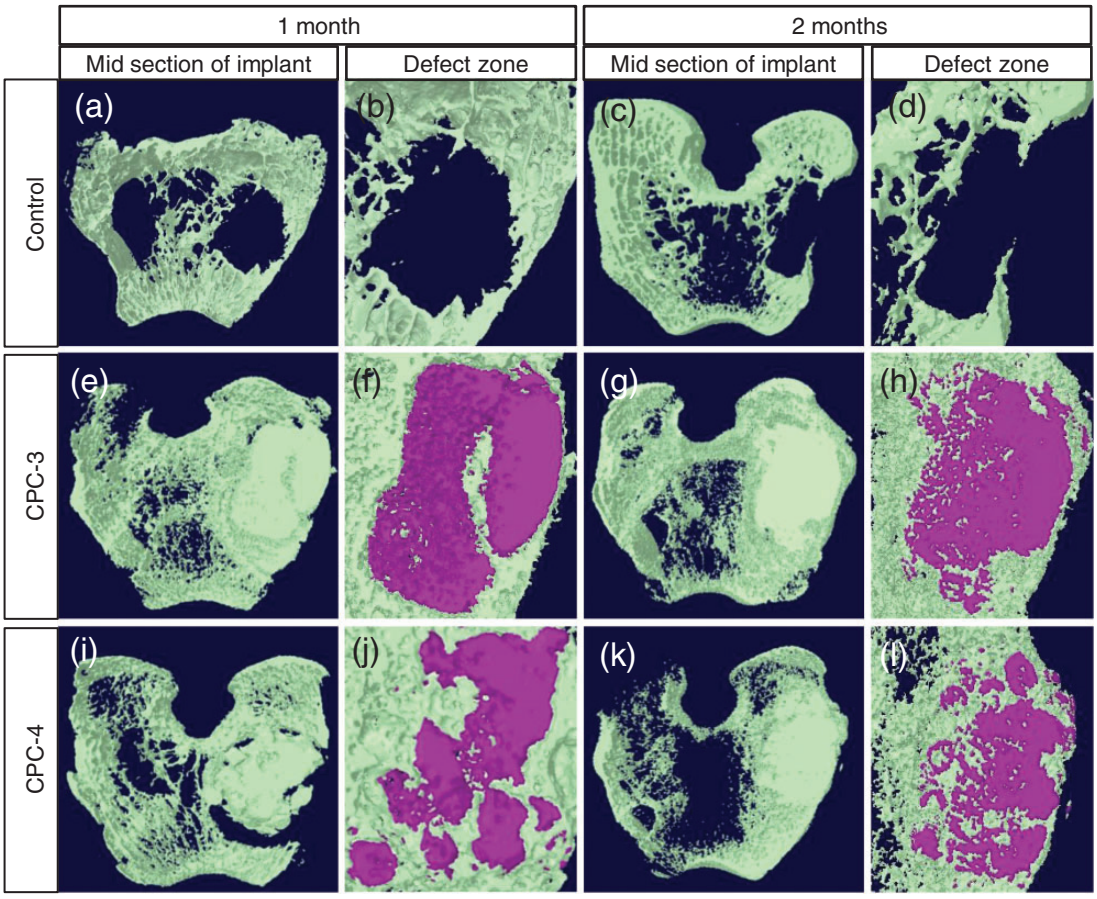

Figure 4. 3D reconstructed micro-CT images of the implanted zone with control after (a, b) 1 month and (c, d) 2 months of plantation. Micro-CT images of the implanted zone with CPC 3 after (e, f) one month and (g, h) two months of implantation. Micro-CT images of the implanted zone with CPC 4 after (i, j) one month and (k, h) two months of implantation.

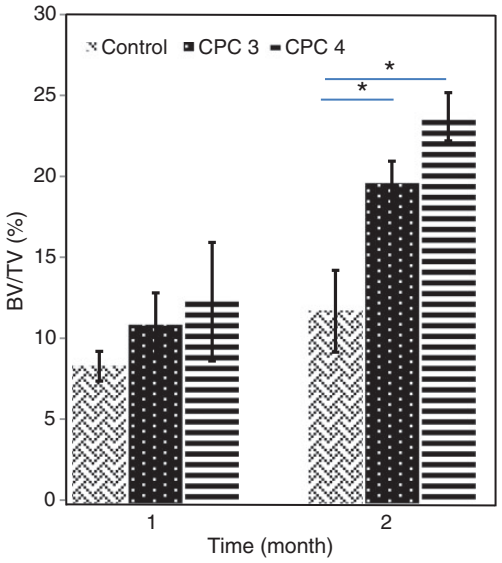

Figure 5. Percentage bone volume formed after one and two months of implantation, computed from the 3D reconstructed micro-CT model.

can significantly improve the bone regeneration behavior of the bone cement.

Histological analysis. SEM observation: SEM images of the polished mid-section of the implant in the defect zone depicting the interface of CPC–new bone and new bone–native bone after two months of implantation are presented in Figure 6. Figure 6(a) and (b) shows low magnification images from CPC3 and CPC4 implanted in femur head. Figure 6(b) and (c) shows corresponding enlarged images from the regions indicated as new bone–old bone interface (N–B) and CPC3–new bone interface (C–N), respectively, from Figure 6(a). Figure 6(f) and (e) shows enlarged images of N–B and C–N from Figure 6(d). Figure 6(e) also shows the interface between the new bone and the Frabone. EDS acquired from the aforementioned regions of the defect area are presented in Figure 6(g) to 6(i).

H & E staining: To investigate the bone formation around the implanted CPC3 and CPC4 in-vivo, decalcified tissue segments were H & E stained. Figure 7(a)

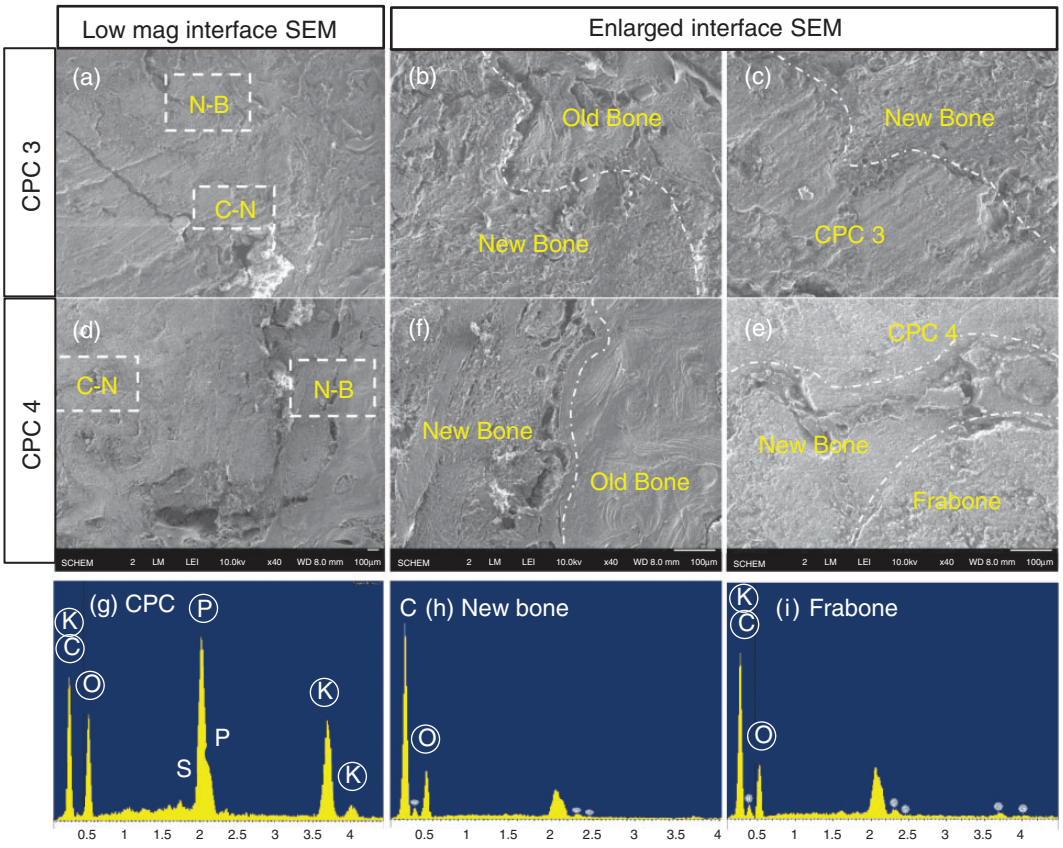

Figure 6. SEM images of the interfacial region of the implanted bone cement. (a) SEM image of CPC 3 and the interface zone with (b) enlarged SEM image from new bone–native bone interface marked by N–B and (c) CPC 3–new bone interface marked my C–N. (d) Interfacial SEM images are shown for CPC 4 with (e) enlarged SEM image from new bone–native bone interface marked by N–B and (f) CPC 4–new bone interface marked my C–N. The EDS profiles of the (g) CPC matrix, (h) new bone, and (i) Frabone are taken to confirm the respective regions. (In EDS profiles: K=Calcium, C=Carbon, O=Oxygen, S=Silicon, P=Phosphorous).

to (c) shows low magnification optical images of control, CPC3 and CPC4 specimens after one month of implantation. Figure 7(d) to (f) shows corresponding enlargements showing the cellular environment of the interface zone. Figure 7(g) to (i) shows low magnification optical image of control, CPC3 and CPC4 after two months of implantation, with corresponding enlargements presented in Figure 7(j) to (l). The control defect showed minimal bone formation at the edge of the defect zone. Inflammatory cells were observed in the defect zone after 1 month and new tissue formation was evident from the active formation zone at the defect-native bone junction. However, the defect micro-environment did not show any significant bone formation activity after 1 month of implantation. CPC3 showed moderate bone formation at the native bone CPC3 interface and did not show any sign of systemic rejection. Lamellar bone formed just behind the collagenous front adjacent to the CPC3. It was evident from the CPC3–tissue interface that the degradation of the CPC was cell-mediated and bone formation occurred from the native bone side and approached inward with the continual degradation of the CPC3. These events were more evident from the two-month H & E stained images (Figure 7(h) and (k)). Multinucleated osteoclast cells were extensive near the CPC3 edge and a sheath of bone forming osteoblast cells lined the newly formed bone. As the cement matrix for the CPC3 and CPC4 was the same, the degradation behavior, and bone formation behavior were similar, as expected, except for the Frabone containing zone of the CPC4. Frabone granules at the edge of the defect zone were exposed to the physiological environment after the initial degradation of the peripheral cement matrix and its channels were open to cellular invasion. After one month of implantation, the porous channels showed the same cellular microenvironment as the adjacent tissue near the interface, without signs of bone formation within. However, after two months of implantation, the pores were fully covered with new bone with extensive lamellar bone formation mimicking the osteon building block. Micro-blood vessels were present at the newly

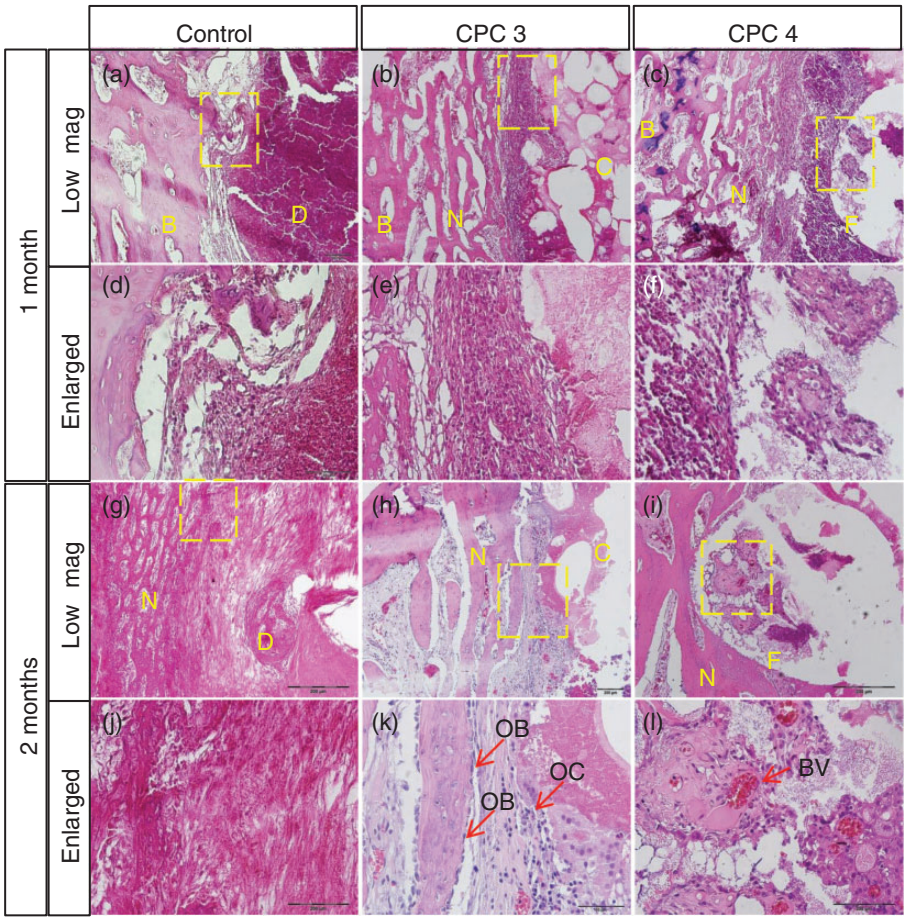

Figure 7. Hematoxylin and Eosin staining of the control and implanted zone tissue section. Low magnification image for (a) control, (b) CPC 3 and (c) CPC 4 after one month of implantation. Corresponding high magnification images of (d) control, (e) CPC 3 and (f) CPC 4 from the selected area. Low magnification images after two months of implantation for (g) control, (h) CPC 3 and (i) CPC 4. Corresponding high magnification images of (j) control, (k) CPC 3 and (l) CPC 4 from the selected area. (B = native bone, D = defect zone, N = new bone formed, F = frabone, C = CPC matrix).

formed bone interface and inside the porous channels. The granules were not degraded within this short time following implantation, as expected, and bone ingrowth advanced inward keeping aside the granules.

Masson's trichrome staining: New bone formation around the implanted CPC3 and CPC4 was further confirmed by Masson's trichrome staining (Figure 8). This stain differentiates between the calcified old bone and newly deposited bone by the presence of collagen type 1. The control samples (Figure 8(a) and (d)) showed sporadic new bone formation after one month of implantation. After two months of implantation, the control specimen did not exhibit any remarkable alteration. However, the interfacial zone in CPC3 after one month of implantation was seen with the presence of blue-stained collagen 1 confirming the new bone formation (Figure 8(b) and (e)). After two months, extensive new bone formation was observed with the CPC (Figure 8(h), and enlarged image in 8(k)). As with the CPC3, CPC4 presented extensive new bone formation (Figure 8(i) and the enlarged image in Figure 8(l)). In CPC4, the Frabone granule interior channels were conducive to new bone formation (Figure 7(i) and (l)). However, inside channels did not show similar bone formation due to the limited or unavailable access. Once the CPC matrix was degraded, bone formation was anticipated to progress gradually. Some residual CPC matrix was left behind the advancing bone–CPC interface (Figure 8(h) and (k)) indicating active cell-mediated degradation of the CPC.

Discussion

Macropores are introduced in a resorbable bone cement to allow cellular ingrowths and increase the surface area available for cell adhesion. These are the first steps in the process of osteoconductivity. The presence of interconnected macro-pores in bone substitutes is probably the most important morphological feature for bone substitute scaffolds that permit successful

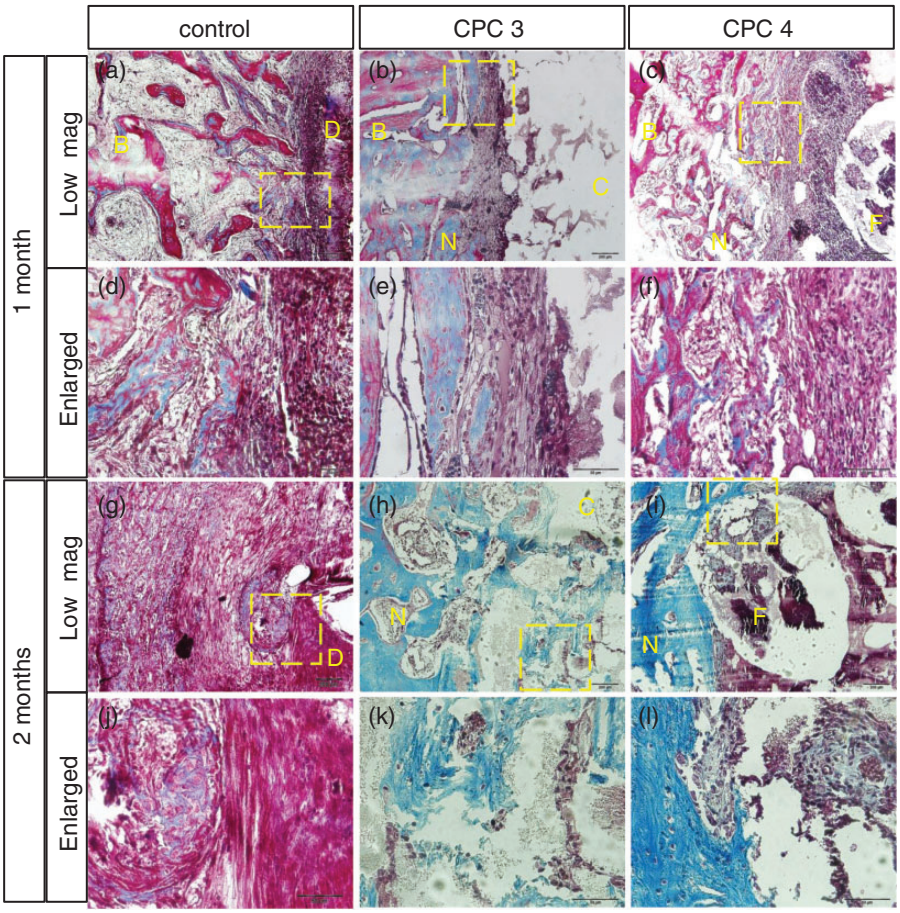

Figure 8. Masson's Tricrome staining of the control and implanted zone tissue section. Low magnification image for (a) control, (b) CPC 3, and (c) CPC 4 after one month of implantation. Corresponding high magnification images of (d) control, (e) CPC 3, and (f) CPC 4 from the selected areas. Low magnification images after two months of implantation for (g) control, (h) CPC 3, and (i) CPC 4. Corresponding high magnification images of (j) control, (k) CPC 3, and (l) CPC 4 from the selected areas. (B = native bone, D = defect zone, N = new bone formed, F = frabone, C = CPC matrix).

and fast bone in-growth. In case of bone cement, although an interconnected macro-porous architecture is highly unlikely, the introduction of randomly distributed macro-pores can significantly improve osteoconductivity by assisting cell in-growth, and enhancing the degradation of the cement matrix. Due to the nature of onsite processing of bone cement by the mixing of different constituent solid and liquid phases, interconnected porosity is unlikely. Fast resorbable porogenic materials have been used as proxies for pore introduction, after which dissolution and removal of the degraded product provides porous space. Cells gain access as the CPC wall resorbs, which separates adjacent isolated pores to obtain effective osteoconductivity. The time required for this step can be shortened by replacing porogen material by well-defined pores, lowering the pore number and increasing the pore length. These are only possible by introducing a secondary porous preform within the cement matrix. However, 1introducing a porous preform can weaken the bone cement. This necessitates a mechanically strong preform to be used in the CPC. The preform size is crucial as larger preform will jeopardize the applicability of the CPC. Thus, incorporating Frabone as a multichannel granular preform in the CPC matrix can significantly improve the cell material interaction with the applied CPC in physiological conditions and improve the osteoconductivity at the same time providing a stable mechanical performance. After a certain period, the brushite CPC is transformed to calcium-deficient apatite, which is much harder to resorb, either by cellular processes or physical degradation. Thus, the free porous interior of Frabone can ensure the cellular in-growth deep inside the implant for further degradation within the implant behind the common interface of CPC and the newly formed bone.

Biocompatibility of the CPC is primarily governed by the material of the CPC matrix. Generally, the

brushite-based cement matrix showed good biocompatibility for bone regeneration application. Thus, chemical modification of the CPC matrix is key to modification of the innate biocompatibility. The addition of silicon in the CPC matrix influences the overall biocompatibility of the system. However, one of the major reasons to modify the CPC composition is to modulate the processing conditions, like optimizing the setting time and applicability (for putty-type CPC like that used in this study) or mechanical performance, such as early strength or higher overall compressive strength. To satisfy these suitable set of parameters, we additionally incorporated nanophase TCP and tri-sodium citrate. The synthesized powder was very reactive and TCP acted as a filler for better packing and, in a sense, as a retarding agent by delaying the setting of the CPC. Sodium citrate and pyrophosphate in the liquid phase acted to delay the setting time; a suitable setting time of 5–7 min resulted. Tri-sodium citrate has a strong ionic group capable of considerably altering the surface charge characteristics of nanoparticles. After the addition of TCP nanoparticles, the consistency of the CPC paste was markedly modified, with the paste becoming very malleable after less than a minute of vigorous mixing. Adsorption of tri-sodium citrate to the nanoparticles increased their surface charge, which significantly reduced the interparticular friction and made the paste malleable. This was favorable for mixing with the subsequent addition of Frabone granules. Due to the high loading of Frabone granules in the CPCs, consistency of the paste decreased. However, it retained its pliability and was useable to apply as putty in bone defect. The particle packing of the set CPCs was excellent (Figure 2e). Densification of the CPCs typically showed considerable micro-porosity, which was responsible for lower mechanical strength. The use of TCP nano-powders and tri-sodium citrate made the solid packing and dense microstructure. The EDS mapping revealed localized concentrations of silicon and sodium. This is because of the presence of sodium in the liquid phase, which tended to concentrate at the surface of particles. The silicon-rich phase predominantly crystallized as $Ca_2(SiO_4)$ phase (Figure 1c).

After mixing, many calcium ions were instantly released and a calcium-rich ionic environment was established in the CPC. Adsorption of the high charge density citrate ions increases the zeta-potential of the particles. Theoretically, the setting reactions of brushite-based cement usually occur via acid–base reactions in situ in the presence of an aqueous phase.[27] Cement formation is based on the different pH-dependent solubility of CPs (HAp or DCPD). When the pH is low, DCPD precipitates. The acidity of the setting cement depends strongly on the nature of the CP salts used, the acidity of the liquid phase reagents, and the reaction rate. When CP salts react in an acidic environment to form cement, it normally involves the dissolution and recrystallization process. Both the extent of initial dissolution and the type of precipitated crystals are controlled by the pH. In that sense, lower pH favor the formation of brushite crystals. But at the same time, this lower pH decreases the biocompatibility of the CPC system which can show the best attributes at physiologically relevant pH 7.4. In our developed CPC system, large release of sodium ion from sodium–silicon–CP played a role in modifying the pH. As shown in Figure 3(c), the initial pH reached a peak that is close to a physiologically relevant value and then slowly decreased. This initial higher pH is crucial for the functioning of relevant cells for attaching on the CPC surface and it is true that the physiological milieu has a strong buffering action for the introduced low pH CPC and eventually factor out any initial immune response. But ensuring a less severe pH definitely improves the cell material interaction in terms of response time of the early onset of osteointegration. This also translated into a better biocompatibility of the samples. The residual DCPD resorbed under physiological conditions, because of much higher solubility at pH 7.4 when compared to HAp. Thus, maintaining a lower pH at the material interface makes sense for faster degradation. This way, the matrix of CPC4 ensures a desirable pH profile. The retardant tri-sodium citrate also acted as a pH buffer ensuring regulation of the pH in a range that was physiologically relevant. However, higher pH for brushite-based systems has a penalty as this would affect the recrystallization and precipitation process and eventually decrease the strength of the set CPC. That is one of the reasons for the lower compressive strength for the fabricated CPC system in this work.

Brushite-based biomaterials are resorbed in vivo to a much larger extent.[28,29] Initial biodegradation of brushite occurs through dissolution, disintegration, and cellular activity.[30–33] Once the microenvironment at the implant interface is over with the initial immune response, the degradation prominently occurred by cellular activity.[34] From the micro-CT image in Figure 4, it is evident that the fabricated brushite cement degraded rapidly. CPC4 with granule loading enhanced the degradation and showed the deep cellular penetration into the implant zone with the support of the channels within the granules. Percentage bone volume data (Figure 5) showed that, compared to the control defect, bone volume was significantly improved in CPC3 and CPC4 two months after implantation.

Brushite cements can be demineralized by osteoclasts cells and enhance the bioresorption.[35] However, macrophage activities are the major contributors for the early onset and regulation of resorption of brushite

cements.[31,36,37] In both instances, the channels through the cylindrical granules loaded in the CPC can aid in the underlining process of degradation by ensuring greater surface area and allowing the cellular ingression deeper inside the implant. Histological analyses of 1 month of implantation revealed macrophage activity near the bone–implant interface (Figure 7(a) to (c) and (d) to (f)). The activity was high after one month and decreased considerably after two months of implantation (Figure 7(g) to (i), and (j) to (l)), although it is safer to say that the macrophage activity is strongly influenced by the extent of foreign body reaction of the implant system and may not be referred to be associated entirely with the biodegradation process. After the initial rapid degradation in vivo, it is reported that brushite cement begins to convert into less-soluble apatite slowing the degradation process.[38] At this point, dissolution of the cement is markedly reduced, and resorption is carried out mainly by osteoclasts activity.[34,37] From the H & E and MT stained images in Figures 7 (h) and (i) and 8 (h) and (i), respectively, multinucleated osteoclast cells are clearly visible adjacent to the implant and newly formed bone with osteoblast cell linings are evident. The channels in the granules are fully covered with new bone adjacent to the interface and are gradually advancing inward with the advancement of the degradation of the CPC matrix. Fully developed blood vessels in the formed bone in the channels confirmed the directional development of bone within the channels.

The results of the in vivo experiments proved that the addition of porous granule positively alters the bone regeneration extent of the CPC by enhancing the inherent degradation of the CPC matrix, which reduces the time for ossification and additionally ensures passage for the osteogenic cells to penetrate deep inside the implant for faster bone in-growth.

Conclusion

Brushite-based CP cement was fabricated with improved degradation and bone regeneration ability by incorporating sodium and silicon in the precursor powder and micro-channeled granules. Faster resorption rate and favorable pH with CPC was found by the addition of silicon and sodium into the synthesized calcium phosphate powder. Compressive strength was not significantly altered, except during the initial week, with the addition of micro-channeled granules. Frabone addition to the CPC provided passage for osteogenic cells for bone in-growth and increased cell-mediated degradation of the CPC. In in-vivo investigation, significantly improved new bone formation was evident due to the presence of Frabone in the CPC matrix. Thus, Frabone-loaded CPCs can be a good alternative for putty-like, instantly applicable bone cement for repairing critical size bone defects.

Declaration of Conflicting Interests

The author(s) declared no potential conflicts of interest with respect to the research, authorship, and/or publication of this article.

Funding

The author(s) disclosed receipt of the following financial support for the research, authorship, and/or publication of this article: The authors extend their special thanks to Reiza Ventur, Department of Regenerative Medicine, College of Medicine, Soonchunhyang University and Mr Jun Ho Lee, Department of Plastic and Reconstructive Surgery, College of Medicine, Soonchunhyang University Hospital for their support in the in-vivo experiment with rabbit model. This work was supported by the Soonchunhyang University Research Fund (No. 20150000).

References

1. Daculsi G. Biphasic calcium phosphate concept applied to artificial bone, implant coating and injectable bone substitute. *Biomater* 1998; 16: 1473–1478.
2. Watson JT. The use of an injectable bone graft substitute in tibial metaphysical fractures. *Orthopedics* 2004; 27: 103–107.
3. Weiss P, Gauthier O, Bouler JM, et al. Injectable bone substitute using a hydrophilic polymer. *Bone* 1999; 25: 67S–70S.
4. Karesh JW. Biomaterials in ophthalmic plastic and reconstructive surgery. *Curr Opin Ophthal* 1998; 9: 66–74.
5. Brown WE and Chow LC. A new calcium phosphate water setting cement. In: Brown PW (ed.) *Cements research progress*. Westerville, OH: American Ceramic Society, 1986, pp.351–79.
6. Constanz BR, Ison IC, Fulmer M, et al. Skeletal repair by in situ formation of the mineral phase of bone. *Science* 1995; 267: 1796–1799.
7. Ooms EM, Wolke JGC, Heuvel MT, et al. Histological evaluation of the bone response to calcium phosphate cement implanted in cortical bone. *Biomater* 2003; 24: 989–1000.
8. Chow LC. Next generation calcium phosphate-based biomaterials. *Dent Mater J* 2009; 28: 1–10.
9. Constantz BR, Barr BM, Ison IC, et al. Histological, chemical, and crystallographic analysis of four calcium phosphate cements in different rabbit osseous sites. *J Biomed Mater Res* 1998; 43: 451–61.
10. Miyamoto Y, Ishikawa K, Takechi M, et al. Histological and compositional evaluations of three types of calcium phosphate cements when implanted in suvcutaneous tissue immediately after mixing. *J Biomed Mater Res* 1999; 48: 36–42.
11. Theiss F, Apelt D, Brand B, et al. Biocompatibility and resorption of a brushite calcium phosphate cement. *Biomater* 2005; 26: 4383–4394.

12. Kuemmerle JM, Oberle A, Oechslin C, et al. Assessment of the suitability of a new brushite calcium phosphate cement for cranioplasty – an experimental study in sheep. *J Cranio-Maxill Surg* 2005; 33: 37–44.
13. Rupprecht S, Merten HA, Kessler P, et al. Hydroxyapatite cement (BoneSourceTM) for repair of critical sized calvarian defects—an experimental study. *J Cranio-Maxill Surg* 2003; 31: 149–153.
14. Wiltfang J, Kessler P, Buchfelder M, et al. Reconstruction of skull bone defects using the hydroxyapatite cement with calvarial split transplants. *J Oral Maxilofac Surg* 2004; 61: 29–35.
15. Sugawara A, Nishiyama M, Kusama K, et al. Histopathological reaction of calcium phosphate cement. *Dent Mater J* 1992; 11: 11–6.
16. Ishikawa K, Takagi S, Chow LC, et al. Behavior of a calcium phosphate cement in simulated blood plasma in vitro. *Dent Mater* 1994; 10: 26–32.
17. Ginebra MP, Fernandez E, De Maeyer EAP, et al. Setting reaction and hardening of an apatite calcium phosphate cement. *J Dent Res* 1997; 76: 905–912.
18. Markovic M, Takagi S and Chow LC. Formation of macropores in calcium phosphate cements through the use of mannitol crystals. *Key Eng Mat* 2000; 192: 773–776.
19. Takagi S and Chow L. Formation of macropores in calcium phosphate cement implants. *J Mater Sci Mater Med* 2001; 12: 135–139.
20. Byun IS, Sarkar SK, Jyoti MA, et al. Initial biocompatibility and enhanced osteoblast response of Si doping in a porous BCP bone graft substitute. *J Mater Sci: Mater Med* 2010; 21: 1937–1947.
21. Carpena NT. *Surface-modification of hydroxyapatite based bone substitutes and evaluation of in vitro and invivo bone studies*. MS Thesis, Soonchunhyang University, South Korea, 2014.
22. Hing KA, Revell PA, Smith N, et al. Effect of silicon level on rate, quality and progression of bone healing within silicate-substituted porous hydroxyapatite scaffolds. *Biomater* 2006; 27: 5014–5026.
23. Pietak AM, Reid JW, Stott MJ, et al. Silicon substitution in the calcium phosphate bioceramics. *Biomater* 2007; 28: 4023–4032.
24. Carlisle EM. Silicon as an essential trace element in animal nutrition. In: Evered D, O'Connor M (eds) *Silicon Biochemistry Ciba Foundation Symposium 121*, London, England, 17–19 September 1985, pp.123–139. Chichester: John Wiley and Sons Ltd.
25. Henstock JR, Canham LT and Anderson SI. Silicon: the evolution of its use in biomaterials. *Acta Biomater* 2015; 11: 17–26.
26. Tran XV, Gorin C, Willig C, et al. Effect of a calcium-silicate-based restorative cement on pulp repair. *J Dent Res* 2012; 91: 1166–1171.
27. Barralet JE, Grover LM and Gbureck U. Ionic modification of calcium phosphate cement viscosity. Part II: hypodermic injection and strength improvement of brushite cement. *Biomater* 2004; 25: 2197–2203.
28. Apelt D, Theiss F, El-Warrak AO, et al. In vivo behavior of three different injectable hydraulic calcium phosphate cements. *Biomater* 2004; 25: 1439–1451.
29. Tamimi F, Nihouannen DL, Eimar H, et al. The effect of autoclaving on the physical and biological properties of dicalcium phosphate dihydrate bioceramics: brushite vs. monetite. *Acta Biomater* 2012; 8: 3161–3169.
30. Frayssinet P, Gineste L, Conte P, et al. Short-term implantation effects of a DCPD-based calcium phosphate cement. *Biomater* 1998; 19: 971–977.
31. Theiss F, Apelt D, Brand BA, et al. Biocompatibility and resorption of a brushite calcium phosphate cement. *Biomater* 2005; 26: 4383–4394.
32. Kuemmerle JM, Oberle A, Oechslin C, et al. Assessment of the suitability of a new brushite calcium phosphate cement for cranioplasty – an experimental study in sheep. *J Cranio Maxillofac Surg* 2005; 33: 37–44.
33. Grover LM, Knowles JC, Fleming GJP, et al. In vitro ageing of brushite calcium phosphate cement. *Biomater* 2003; 24: 4133–4141.
34. Grossardt C, Ewald A, Grover LM, et al. Passive and active in vitro resorption of calcium and magnesium phosphate cements by osteoclastic cells. *Tissue Eng A* 2010; 16: 3687–3695.
35. Xia ZD, Grover LM, Huang YZ, et al. In vitro biodegradation of three brushite calcium phosphate cements by a macrophage cell-line. *Biomater* 2006; 27: 4557–65.
36. Constantz BR, Barr BM, Ison IC, et al. Histological, chemical, and crystallographic analysis of four calcium phosphate cements in different rabbit osseous sites. *J Biomed Mater Res* 1998; 43: 451–461.
37. Bohner M, Theiss F, Apelt D, et al. Compositional changes of a dicalcium phosphate dihydrate cement after implantation in sheep. *Biomater* 2003; 24: 3463–3474.